RSC Advances



This is an *Accepted Manuscript*, which has been through the Royal Society of Chemistry peer review process and has been accepted for publication.

Accepted Manuscripts are published online shortly after acceptance, before technical editing, formatting and proof reading. Using this free service, authors can make their results available to the community, in citable form, before we publish the edited article. This Accepted Manuscript will be replaced by the edited, formatted and paginated article as soon as this is available.

You can find more information about *Accepted Manuscripts* in the **Information for Authors**.

Please note that technical editing may introduce minor changes to the text and/or graphics, which may alter content. The journal's standard <u>Terms & Conditions</u> and the <u>Ethical guidelines</u> still apply. In no event shall the Royal Society of Chemistry be held responsible for any errors or omissions in this *Accepted Manuscript* or any consequences arising from the use of any information it contains.



Covalent modification of graphene oxide by metronidazole

for reinforce anti-corrosi on of epoxy coatings

Zongxue Yu a,1, Liang Lv a, Yu Ma a, Haihui Di a, Yi He a, b,2,

a Southwest Petroleum University, School of Chemistry and Chemical Engineering, Chengdu, 610500, China.

b State Key Lab of Oil and Gas Reservoir Geology and Exploitation, Chengdu, 610500, China.

Abstract: Graphene can be used as an excellent protection material because of its barrier properties. This work reports a promising application of metronidazole (MET) modified graphene oxide (GO) composites (GME) for the corrosion protection of steel. The composites were synthesized by using the carboxyl of GO and hydroxyl of MET with the help of Maleic anhydride (MA), and dispersing the sheets into epoxy resin at a low weight fraction of 0.2.wt %. The UV-absorption spectrum reveal that MET can be detected in the NaCl (3.5 wt. %) solution. The electrochemical impedance spectroscopy (EIS) test show that the corrosion resistant performance is significantly enhanced by the addition of GME hybrids to epoxy than GO. The scratched test illustrate that less of corrosion products formed in the scratch of steel coated by GME. The strategy of corrosion inhibitor modified graphene oxide can be extended to develop new graphene-based materials with other excellent materials for the protection of metal components.

Keyword: Graphene oxide, Metronidazole, Corrosion coating, Anti-corrosion.

1. Introduction

Recently, graphene has attracted tremendous interest for its unusual physic-chemical properties and possible application in various fields[1,2], such as catalysis[3], biosensors[4], water purification[5,6], etc. However, graphene is a promising candidate for anti-corrosion coating, due to its unique properties, e.g [7-9]. The Nobel Prize Laureate Novoselov K.S. has shown that the inertness and impermeability of graphene can be used as a protective coating through the in situ grown[10]. Singh et al. proved that graphene oxide-polymer composite coating is an effective protective shield for oxidation and corrosion of metal[11]. In our previous study has demonstrated that the corrosion protection properties of the nano-graphene/epoxy composites lays on the metal surface are capable of enhancing the corrosion protection of pure metals effectively [12,13]. With the complication of corrosion environment, the simple coating can not provide the protection, needlessly. It is necessary to study an active protection in addition to the time-limited passive protection. One of the most promising approach to develop more effective anti-corrosion coating is based on use of corrosion inhibitor. Several systems has been confirmed: microcapsules, porous microparticles or stratified layers made of pH sensitive polyelectrolytes[14-18]. Frederico et al. Maia study a nano-container based on silicon package MBT and the result show that the release amount of MBT is effected by the different concentration of pH and Cl⁻[19]. N. Pirhady Tavandashti et al. introduce inorganic corrosion inhibitor into SiO₂/epoxy and add to boehmite, the test demonstrates that cerium nitrate can release from the defects of coating and provide the protection for the metal[20].

Corresponding author.

¹ Zongxue Yu job title: Associate Professor, work units: Southwest Petroleum University, Tel: (+86) 15208397092, fax: (+86) 028-83037315, email:haiqingy@163.com.

² Yi He, Tel.: job title: Associate Professor, work units: Southwest Petroleum University, Tel: (+86) 13881958071, fax: (+86) 028-83037315, email: heyi@swpu.edu.cn.

Polymer epoxy coating is an effective and simple approach for anti-corrosion. But there are defects in the process of epoxy coating solidify, such as micro-pores, bubbling et al[21]. Thus, in order to overcome the this disadvantage, our communication focus developing a route to prepare a covalent modification of graphene oxide by metronidazole(MET)[22] as illustrated in Fig. 1. Via a versatile grafting-to process, maleic anhydride (MA) is grafted onto GO surface utilizing hydroxyl and epoxy bond addition reaction for increasing the content of carboxyl, which come from GO and MA(GM), respectively. In a subsequent step, the covalent attachment of MET onto the modified GM was accomplished by the esterification mechanism (GME). The full test about composite epoxy coating are examined.

2. Experimental methods

2.1. Materials

Deionized (DI) water was produced by a water purification machine (UPC-III-40L, Ulupure), natural graphite powder was purchased from Chendong Organic Chemicals. 4-(dimethyl amino) pyridine (DMAP), dehydrated N,N-dimethylformamide (DMF), maleic anhydride (MA), Metronidazole (MET) and dicyclohexylcarbodiimide (DCC) were purchased from Kanto Chemical Co, Inc. Concentrated sulfuric acid (98%), potassium permanganate (KMnO₄), sodium nitrate (NaNO₃), hydrogen peroxide aqueous solution (30%), anhydrous ethanol (analytical reagent grade), hydrochloric acid (HCl), and sodium hydroxide (NaOH) were obtained from Chengdu Kelong Chemical Reagent Factory.

2.2 The preparation of GO

Graphene oxide (GO) was synthesized by the modified Hummers method[23]. In concise, at low-temperature stage, 0.8 g of graphite was mixed with 24 mL concentrated H_2SO_4 by ultrasonication for 20 min, and then turned the mixture to be in ice bath for half an hour. 1 g NaNO₃ was added into the mixture within 35 min to maintain the temperature of the mixture not exceeding 5 $^{\circ}$ C. KMnO₄ (4.8 g) was mixed slowly in small portions to keep the reaction temperature below 5 $^{\circ}$ C, being followed by stirring for 2 h. Then the mixture was heated up to 39 $^{\circ}$ C and stirred for 2.5 h. Followed by the addition of 41 mL of DI water, the reaction temperature was raised to 95 $^{\circ}$ C for 1.5 h. And 120 mL of 10% H_2O_2 were added to the mixture for one hour. After these, HCl (10%, 100 mL) was taken part in the solution to remove metal ions. Finally, the oxidation was separated by centrifuge and washed with aqueous ethanol. The obtained product was exfoliated through ultrasonication for 4 h, dried at 60 $^{\circ}$ C under vacuum for 12 h and grinded for powder.

2.3 Modification and Graft of the graphene oxide (GO)

Subsequently, 0.3541 g GO and MA(0.073mol) was mixed in a 250 mL round-bottomed flask with stirring and maintained at 75 $^{\circ}$ C for 3 h, and then at 85 $^{\circ}$ C for 16 h. From some study[24] shows that the content of hydroxyl is more than carboxyl's, but this research focus on the carboxyl. We design to modify hydroxyl with MA[25] to improve the content of carboxyl (Fig. 1). The modified product was named GM and it was obtained by drying the residue in the bag at 60 $^{\circ}$ C.

The intentional material (GME) was synthesized according to the similarly reported method[26], as is shown in Fig. 1. A typical synthetic procedure is as follows: To a solution of GM (0.236 g) and MET (5.9mmol) in DMF (50 mL) were added DCC (2mmol) and DMAP (0.04mmol). After the solution was stirred at 80 $^{\circ}$ C for 48 h under a nitrogen atmosphere, the reaction mixture was cooled to room temperature and filtered. The filtrate was evaporated in vacuum, washed with hexane (50 mL), and then dried at 100 $^{\circ}$ C in vacuum for 24 h to give GME as a viscose liquid.

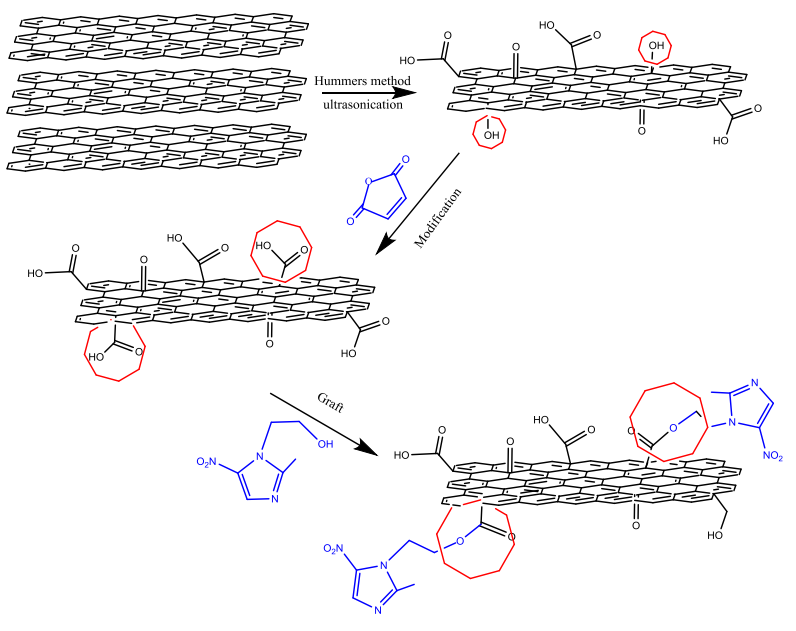


Fig. 1 Flow chart for the synthesis of GME hybrid material

2.4 Preparation of composite coatings

To prepare the coatings mixture, the epoxy resin was accompanied by a known amount of Nano filler (0.2 wt. % mass fractions of GO, GM and GME). The mixture was sprayed on the steel surface after the ultrasonic oscillation and mechanical stirring of the redundant mixture into a homemade container. The steel with coating and the redundant mixture were torrefied at 120 $^{\circ}$ C for 60 min, followed by drying at 220 $^{\circ}$ C for 90 min in an oven[27]. And the cured epoxy coating were named pure epoxy coating, GO epoxy coating and GME epoxy coating, respectively.

2.5 Structure and Electrochemical characterization

The obtained GO, GM and GME sample was characterized by FT-IR, XRD, TGA, XPS, UV, and SEM. Thermo Gravimetric Analyzer (TGA) and Fourier transform infrared (FT-IR) spectroscopy spectra was recorded on a DSC1-1100L (METTLER, Switzerland) in the range of 50–800 °C and on a WQF 520 spectrometer in the range of 500–4000 cm-1. X-ray diffraction (XRD) analysis (X'Pert PRO MPD, Holland) was used to identify the crystallinity of the composite with a voltage of 40 kV and a generator current of 20 mA was used. The scanning rate was 1.5 °min and scanning rage was about 5 °-80 °. X-ray photoelectron spectra (XPS) were recorded on an XSAM 800 photoelectron spectrometer (KRATOS) with Al Ka (1486.6 eV) as the Xray electric current set at 12 mA and the High Voltage at 12 kV, C1s (284.8 eV) corrected electron binding energy values. The solid-state 13C NMR experiments were carried out on Agilent DD2-600 MHz NMR spectrometer.

The measurement of corrosion inhibitor release from GME was performed in neutral, adjusted by NaCl. In this work, 0.005 g GO, 0.005 g pure MET and 0.005 g GME powders were submerged in the 25 mL NaCl (3.5 wt.%) solution for 84 h. The solutions was filtrated by pumping membrane filter. The filtrated solutions and NaCl (3.5 wt. %) pure solution were characterized by UV–vis spectrometer (UV-1800, Shimadzu).

Electrochemical impedance spectroscopy (EIS) measurements were investigated by the electrochemical workstation (EIS, CHI604D, China) at 104–10⁻¹ Hz with a sine wave signal amplitude of 100–10 mV[28].

3. Results and discussion

3.1 Characterization of GO, GM and GME

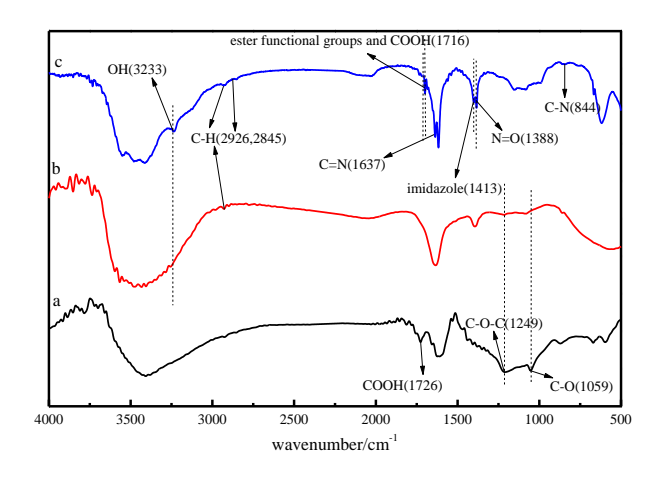


Fig. 2. The FT-IR spectrum of GO (a), GM (b) and GME (c).

The containing groups on the surface of GO, GM and GME are characterized by FT-IR analysis (Fig. 2). Different functional groups are found in the FT-IR spectrum and it exhibits several characteristic peaks of O–H at 3407 cm⁻¹, COOH group at 1726 cm⁻¹, C=C at 1623 cm⁻¹, C=O–C group at 1249 cm⁻¹, C=O group at 1059 cm⁻¹. It is indicated that abundant oxygen-containing functional groups exist on the surface of GO Nano-sheets. The absorption peaks at 1394 cm⁻¹ may be associated to the COOH stretch in MA. Different functional groups of GME are found in the FT-IR spectrum (Fig2c). For MET, bands[29,30], are assigned to OH stretching (3233 cm⁻¹), C=N stretching (1637 cm⁻¹)[22], N=O stretching (1388 cm⁻¹), C=NO₂ stretching (844 cm⁻¹) and the related C-H(2926, 2845 cm⁻¹). It's not obvious different between ester functional groups and COOH at 1716 cm⁻¹[31-33]. The peak of 1413 cm⁻¹ is duo to the imidazole ring[31]. All results show that preparation of GME is successful.

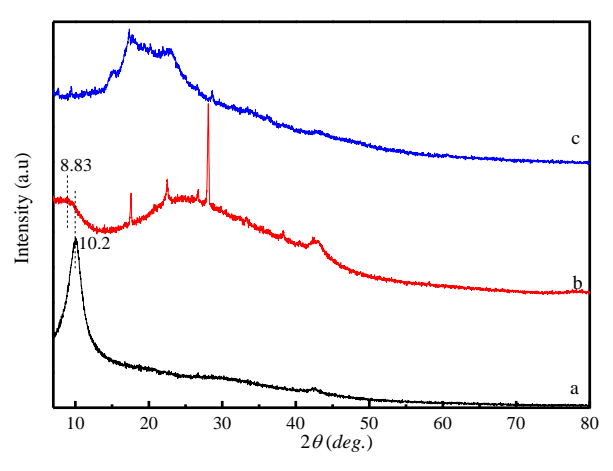


Fig. 3. The XRD spectrum of GO (a), GM (b) and GME (c).

The XRD patterns of the GO, GM and GME have been shown in Fig. 3. As shown of Fig. 3-a, the GO has an intense crystalline peak at 10.2 °, corresponding to a d-space of 0.886nm, The interlayer spacing of GO sheets can be attributed to its oxygenated functional groups introduced by the modified Hummers method. The XRD of the GM as showing in the Fig. 3-b, and the peak of GO weaken. The peak of GO is at 8.83 ° and the d-space of 1.001nm, which is larger than that of GO due to the introduction of MA[35]. The results of d-space demonstrates modified success. Compared to GM, the XRD of GME (Fig. 3-c) could be clearly observed that the amorphous of

MET exists, but the character of MA disappear. It could confirm that the MET is grafted on the GM and instead of a simple physical mixture.

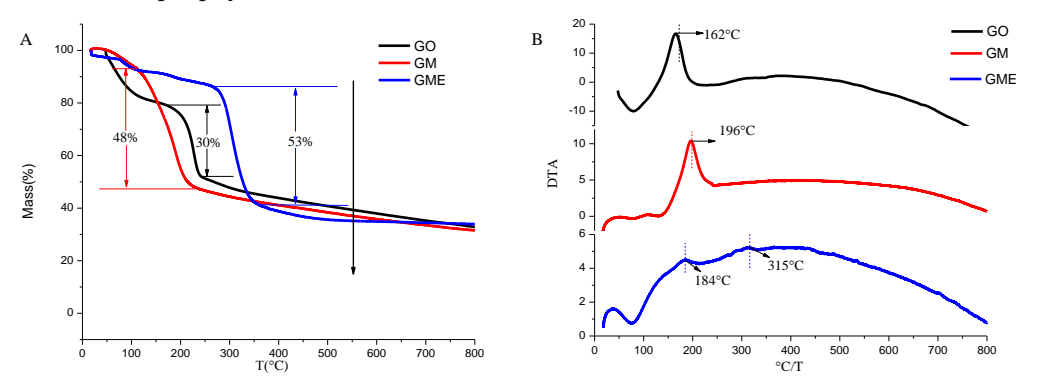


Fig. 4. (A) TG and (B) DTA spectrum of GO, GM and GME

The structural differences between GO, GM and GME are evident from the results obtained by thermogravimetric analysis (TG) and differential thermal analysis (DTA) in Fig. 4. The TG curve of GO (Fig.3A) exhibited three obvious steps of mass loss as literature[36], the weight loss before 100° C is caused by the release of trapped water in these materials. The weight loss of GO starts from 200° C to 260° C (corresponding to a weight loss of GO is about 30%), indicating that there are abundant oxidative groups, corresponding to an obvious exothermic DTA peak (Fig.3B) at 165° C. In comparison, the TG curve of GM (Fig.3A) displays more weight loss than GO, which means it has enhanced the groups in the sheet of GO by MA (Fig.3B) and the exothermic peak is at 196° C (corresponding to the weight loss of GM is about 48%). However, the curve for the GME (Fig.3B) exhibited two steps of mass loss and indicated two weak exothermic peaks at 184° C and 315° C, respectively. It suggested that GO was more groups by grafted MET and enhanced the weight loss of the material.

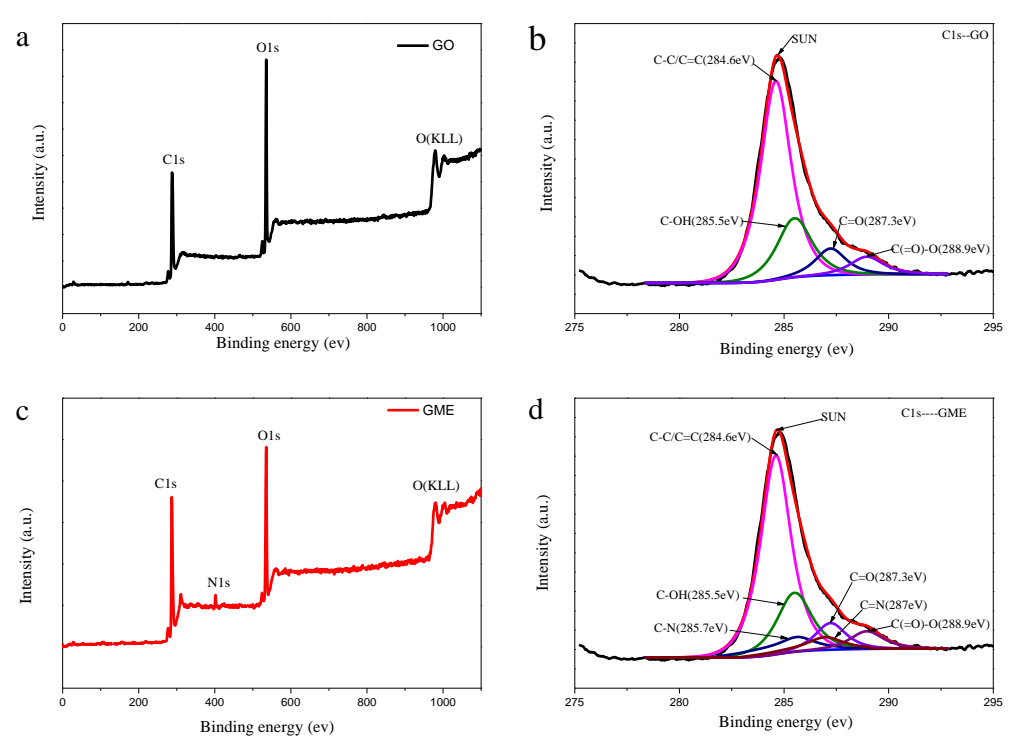


Fig. 5. XPS results and the related C1s spectrum of GO (a, b) and GME (c, d).

The surface chemical compositions and differences between GO and GME are employed by

XPS spectra. As shown in Fig. 5a, the main composition of GO are C and O, and the two typical peaks at ~286.4eV and ~534.8eV, respectively. In contrast, new peaks at ~401eV appear in the XPS spectra of GME (Fig. 5c); the C/O atomic ratio value of GME calculated from the percentages of C1s to O1s show a slight increase (from ~0.986 in GO to 1.555 for GME), which are attributed to the fact that MET chains possess high content in their structures (Fig. 1).The C1s level spectrum of GO with peak-fitting curves in Fig. 5b shows four typical chemically shifted components[37]: C-C/C=C(284.6eV), C-O(285.7eV), C=O(287.3eV), C(=O)-O(288.9eV). After MET modification, appearance of C-N and C=N are observed in the C1s XPS spectra (Fig. 5c and d), implying a reaction between MET and GO. Compared with the GO and GME exhibits a significant increase in the N peak, as shown in Fig. 5c. Moreover, the C1s XPS spectra of GME in Fig. 5d present peaks at ~285.7eV and 287eV, which are assigned to C-N and C=N, respectively. These above mentioned XPS results further demonstrate that GME is successfully preparation, which agrees well with FTIR and XRD.

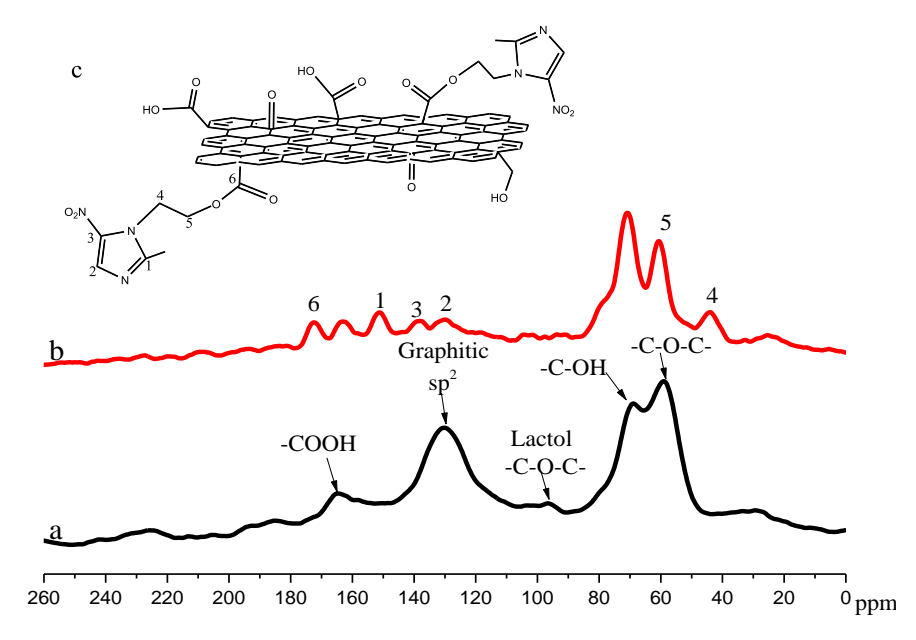


Fig. 6. The ¹³C NMR spectrum of GO (a) and GME (b). Schematic representation of GME (c) with the used labelling of C atoms

In order to differentiate the structure of GME nanofibers in the composite, the solid-state 13C NMR spectra of GO and GME were collected and shown in the Fig.6. The typical resonances of GO are shown in the Fig.6(a), which are ascribed to the epoxy and hydroxyl, and the intense peak at 130 ppm is assigned to the graphitic carbons in the GO[38,39]. However, the solid-state 13C NMR spectrum of GME not only has the typical resonances of GO, but also there are other resonances in the 13C NMR spectrum of GME (Fig. 6(b)). The schematic representation of GME with the used labelling of C atoms is showing in Fig.6(c). In the 13C NMR spectrum of GME, the signals at 172.29, 151.62, 138.23, 130.02, 60.58 and 44.05 ppm are attributed to the C-6, C-1, C-3, C-2, C-5 and C-4 of the presence MET on the GO, respectively. This results indicates that the MET is indeed graft the GO. And the analysis results of 13C NMR is consistent with the results of FT-IR, XRD, TG, and XPS analyzes.

3.2 Release properties of GME

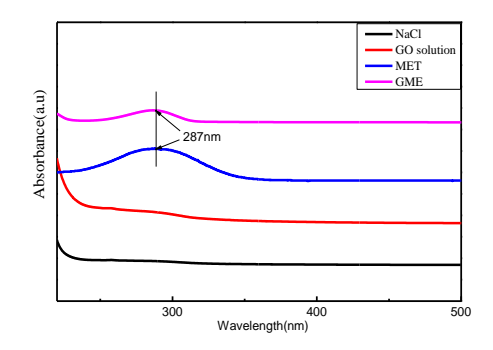


Fig. 7. The release of corrosion inhibitor from GME in NaCl (3.5%wt) solution

Fig. 7 illustrates the release of MET from GME in the NaCl (3.5wt. %) solution with 84 h. As this figure 7 shows, there is not maximum absorption peak in the GO and NaCl solution, but a maximum absorption peak appears at 287nm in the MET solution, indicating the maximum absorption peak of the MET is here. As presented in Fig. 6, the absorption spectrum of GME in the solution has a maximum absorption peak at 287nm, which has been explained that the MET releases in the NaCl solution from the GME material. As a result, it is expected that the mechanical property of the MET release could be attributed to the fracture of grease key in the solution from the GO sheet. In addition, the released property of GME can enhance the anti-corrosion performance when the GME/epoxy coating is broken.

3.3 Thermal stability analysis of composites coating (TG-DTG)

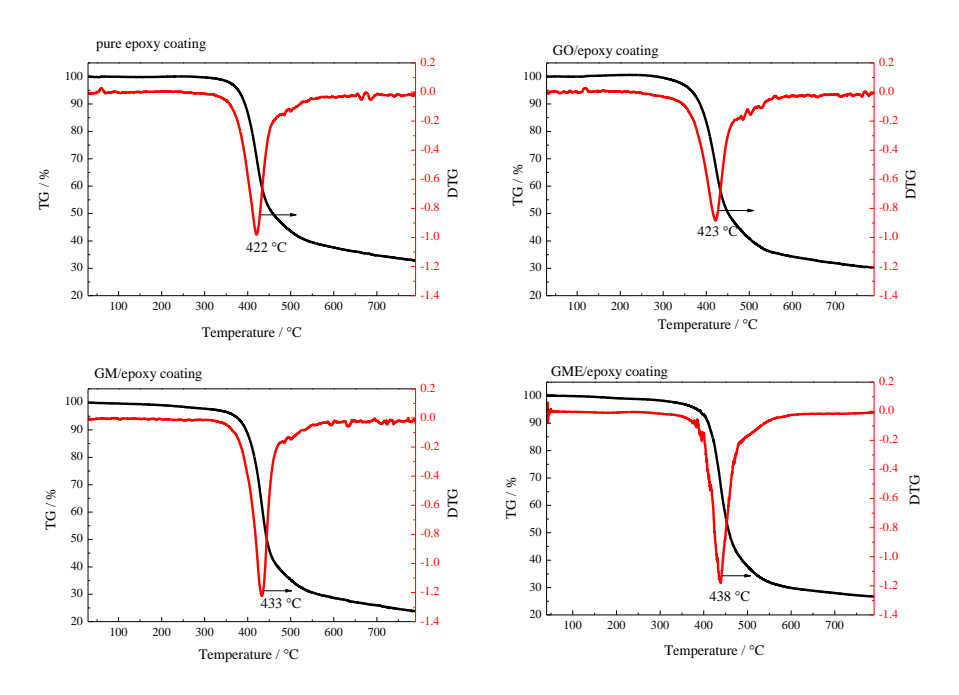


Fig. 8. The TG and DTG curve of the composite coating

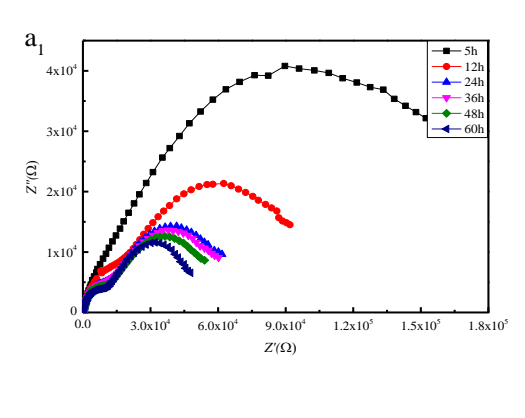
The thermal weight loss curve of composite coating is showing in Fig. 8. The thermal degradation rate of GME/epoxy is higher than others coating, such as the thermal degradation rate of pure epoxy, 0.2 wt. % GO/epoxy, 0.2 wt. % GM/epoxy and 0.2 wt. % GME/epoxy are 67.208%, 69.841%, 76.373% and 77.879%, respectively. According to Table 1, the thermal weight loss of pure epoxy, GO/epoxy, GM/epoxy and GME/epoxy are 56.470%, 59.069%, 64.729% and 62.267%, respectively, at 500°C. The pure epoxy have the least thermal degradation rate, whereas GM epoxy

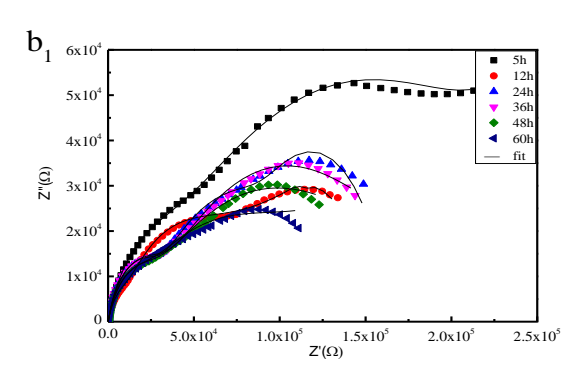
is most, this can contribute to a lot of oxygen-containing functional groups in GO. The thermal degradation rate shows the same tendency at 600 °C. However, the thermal degradation rate of GME/epoxy is the most at all, at 800 °C, this can contribute to some groups have disappeared in the reacted process, so the thermal conductivity of GO is enhanced and the thermal degradation rate of GME/epoxy is highest. From the DTG as showing in Fig. 7, the decomposition temperature of pure epoxy, GO/epoxy, GM/epoxy and GME/epoxy are 422 °C, 423 °C, 433 °C, and 438 °C, respectively. The result because of GO of less groups can improve the thermal conductivity of epoxy, this is consist of TG. The result shows that the thermal stability of composite coating is improved in the GME/epoxy coating.

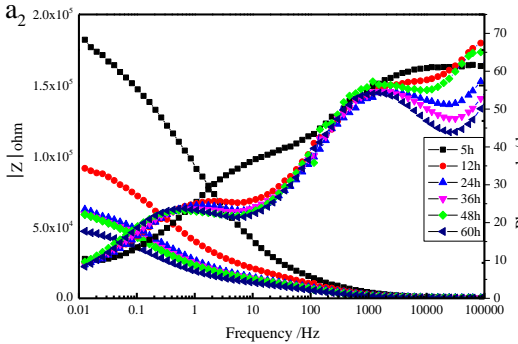
Table 1 Different thermal degradation temperature of composite coating.

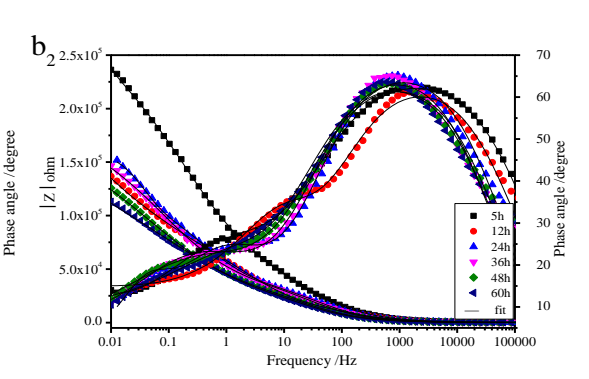
Weight Loss/% Temperature/°C Coatings	350℃	450℃	500°C	600°C	800°C
MET-GO/epoxy	2.874%	44.368%	62.267%	70.141%	77.879%
GM/epoxy	3.438%	53.712%	64.729%	71.366%	76.373%
GO/epoxy	3.118%	49.615%	59.069%	65.726%	69.841%
Pure epoxy	1.653%	48.030%	56.470%	62.411%	67.208%

3.3 EIS studies









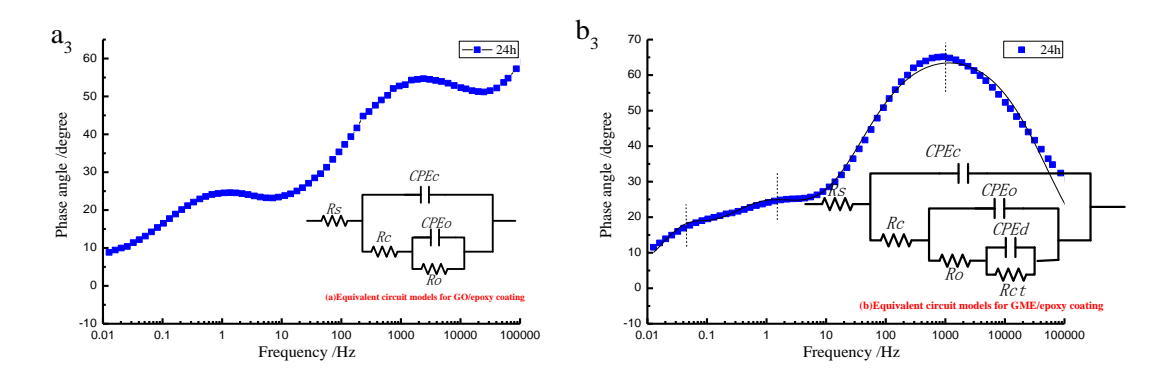


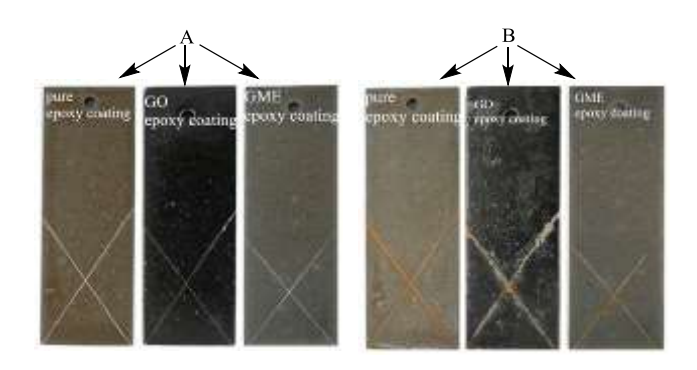
Fig. 9 Equivalent circuit models used for numerical simulation of the EIS measurements of the coatings at different soaking stages (a, b); a: 0.2 wt. % GO/epoxy; b: 0.2 wt. % GME/epoxy; (a₁, b₁,) Nyquist and (a₂, b₂,) Bode diagrams of diffident time (Z': The real part of the impedance, Z": Imaginary impedance, |Z|: impedance module value), (a₃, b₃,) Phase angle diagrams of 24h.

EIS is one of the effective and powerful techniques for the investigation of the corrosion resistance of the coating. In this work, the Nyquist, Bode plots and Phase angle diagrams of 24h for the 0.2 wt. % GO/epoxy coating and 0.2 wt. % GME/epoxy coating during 60h immersion in 3.5 wt% NaCl aqueous solution (Fig. 9). For quantitative estimation of the anti-corrosion resistance of the composites coating, experimental impedance spectra are fitted using equivalent circuits. For the equivalent circuits depicted in Fig. 9(a, b), R_s accounts for the solution resistance; Rc, R_o and Rct can be assigned respectively to the pore resistance of the coating, resistance of the intermediate oxide layer and charge transfer resistance. CPEc, CPEo and CPEd are the constant phase elements of the coating, oxide and double layer, respectively.

The barrier effect is one of the important feature associated with the corrosion protection by organic coating. Therefore, the barrier properties of the coating system can not compromise by the modification of the coatings with GO loaded with MET. The Nyquist of GO/epoxy coating shows that the impedance of GO/epoxy coating is decreasing with the prolonger of immerse time (Fig 9a₁). The corresponding Bode plots are illustrated in Fig. 9a₂ for GO/epoxy coating. It shows that the impedance of low frequency range is also decreasing. The two time constants (high frequencies: $10^{1} \sim 10^{5}$ Hz) is a characteristic for some systems the high frequency range (Fig. 9a₃).

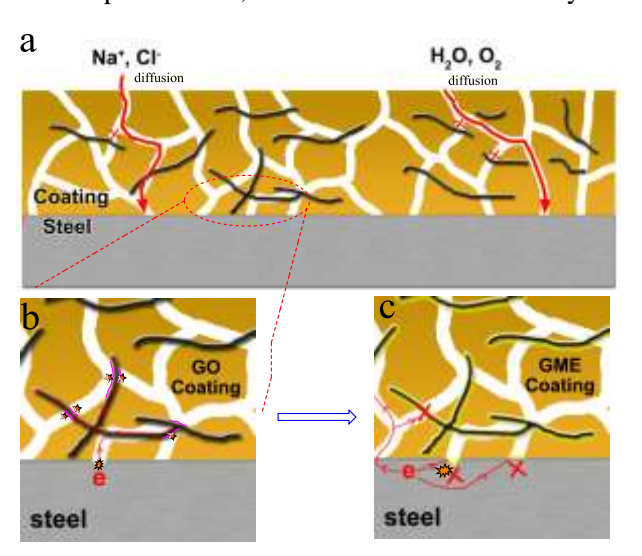
However, protection properties of GME/epoxy coating is slowly degradation with time, then upgrade of GME/epoxy coating the impedance of low frequency with time is due to the exist of MET (Fig. 8b₁ and b₂). The exist of epoxy coating defects can improved the aisle for some molecules (H₂O, O₂ and Cl⁻) to penetrate the coating and the steel substrate will be corroded. Usually, the impedance moduli at low frequencies also reflect the protective properties of coatings. The phase of GO/epoxy coating is the normal propertied of polymer coating, but the GME/epoxy coating is disagree with GO/epoxy coating at low frequency. At low frequency, there is a peak of GME/epoxy coating in Fig.8b₃, indicating that this coating exhibited a good barrier property against corrosive species. This time constant is the responses of metal and reflects the corrosion behavior of metal substrate. This result demonstrates that the anti-corrosion performance of GME/epoxy coating is successful and outstanding.

3.4 Self-healing properties of the scratched specimens



 $\textbf{Fig. 10} \ \ \text{Visual performances of the coatings exposed to NaCl (3.5\% wt) solution \ test for \ 84\ h\ (A: before, B: after)$

The anti-corrosion performance of the multiplex epoxy coating loaded with different addition materials were tested in NaCl (3.5 wt. %) solution test chamber for 84 h in Fig 10. According to Fig 10, it can be clearly seen that corrosion products formed near scribes of all coatings. The accumulation of corrosion products near the scribes was more pronounced on the coating without any addition materials. However, there were some corrosion products in the GO epoxy coating, which was better anti-corrosion performance than pure epoxy coating. Even the epoxy coating within GME was the best performance of anticorrosion. As the Fig 10 shows, the corrosion products which existed in the scribes of GEM epoxy coating were rare. As a result, it is clear from the figure that addition of GME to the coating caused the decrease in the amount of corrosion products produced near the scribes. It also figures out that the grease key that MET grafted to GO sheet in NaCl (3.5wt.%) solution was broken, then the MET could release from the GME and bring into playing an anti-corrosion role to protect steel, which has been illustrated by EIS in 3.3.



The schematic diagram of anti-corrosion process is shown in Fig. 11. There are some oxygencontaining functional groups, such as hydroxy, epoxy and carboxyl, which have proofed by FTIR (Fig. 1) in the GME, so that GME can perfectly disperse in the epoxy coating as Fig. 11-a. Though the addition of GO increases the molecule diffusion resistance in coating matrix, some molecules (H₂O, O₂ and Cl⁻) can penetrate through the GO matrix over a long time scale (Fig. 11). A part of molecules via coating and get the substrate, the steel substrate will be corroded. Some study[40] show that GO and steel expose to corrosive electrolyte, leading to the galvanic corrosion of steel. GO connect with substrate by directly or indirectly, which greatly increase the cathode-to-anode area ratio (Fig. 11a and b). The GME/epoxy coating can prolong the use time of steel, which due to the MET cover on the surface of GO and reduce the conduction of GO. For GME as shown in Fig. 10c, the surface of steel occur corrosion reaction, such as electrochemical oxidation reaction and oxygen reduction reaction. The corrosion reaction are greatly inhibited, which due to the mass transfer is greatly limited by coating, leading to the excellent anticorrosion performance of GME/epoxy coating. And the expose of GME can release MET and format adsorption film on the substrate to protect the steel. The anticorrosion mechanism of GME/epoxy coating is the same as other study[41-43].

4. Conclusions

We have synthesized fine metronidazole grafted graphene oxide nanocomposites via a simple two-step modification and graft without using any extra templates or surfactants. The characteristic functional groups, such as COOH, C=N, N=O, C-NO₂, of modification and graft of GO had been proved by the FTIR, XPS and 13C NMR. The weight loss of GO, GM and GME were 30%, 48% and 53% by TGA, respectively. The thermal weight loss curve of composite coating had confirmed that the GME/epoxy modified the thermal stability of composite coating. Comparison with GO reported in this literature indicated that GME hybrids displayed an obvious advantage in enhancement corrosion resistance and enhanced epoxy coatings' corrosion resistance at a low content (0.2 wt. %). There are several reasons for superiority of the hybrids, which include the release of MET from GME, sheet structure, and the excellent exfoliation in epoxy resin. These results had been consistent with the original design ideas. The scratched specimens could be self-healing where the coating was damaged to prolong the life time of metallic. Herein, the GME hybrids presented a "smart" application in the field of the nanofillers for anticorrosive epoxy coatings.

Acknowledgment

The authors gratefully acknowledge the financial support from the majorly cultivated project of sci-tech achievements transition (15CZ0005) from the education department in Sichuan Province.

References

[1] N. Levi-Polyachenko, D. Carroll, J.I.V. Stewart, Applications of Carbon-Based Nanomaterials for Drug Delivery in Oncology, in: F. Cataldo, T. Da Ros (Eds.) Medicinal Chemistry and Pharmacological Potential of Fullerenes and Carbon Nanotubes, Springer Netherlands, 2008, 223-266.

[2] Z. Zhu, L. Garcia-Gancedo, A.J. Flewitt, H. Xie, F. Moussy, W.I. Milne, A Critical Review of Glucose Biosensors Based on Carbon Nanomaterials: Carbon Nanotubes and Graphene, Sensors, 2012, 12: 5996-6022.

- [3] R. Leary, A. Westwood, Carbonaceous nanomaterials for the enhancement of TiO2 photocatalysis, Carbon, 2011, 49: 741-772.
- [4] W. Yang, K.R. Ratinac, S.P. Ringer, P. Thordarson, J.J. Gooding, F. Braet, Carbon Nanomaterials in Biosensors: Should You Use Nanotubes or Graphene?, Angewandte Chemie-International Edition, 2010, 49: 2114-2138.
- [5] J. Xu, L. Wang, Y. Zhu, Decontamination of Bisphenol A from Aqueous Solution by Graphene Adsorption, Langmuir, 2012, 28: 8418-8425.
- [6] J. Xu, Y.-F. Zhu, Elimination of Bisphenol A from Water via Graphene Oxide Adsorption, Acta Physico-Chimica Sinica, 2013, 29: 829-836.
- [7] J.C.T. Dhiraj Prasai, Robert R. Harl, G. Kane Jennings, and Kirill I. Bolotin, Graphene Corrosion-Inhibiting coating, ACS NANO 2012, 6: 1102-1108.
- [8] K.-C. Chang, M.-H. Hsu, H.-I. Lu, M.-C. Lai, P.-J. Liu, C.-H. Hsu, W.-F. Ji, T.-L. Chuang, Y. Wei, J.-M. Yeh, W.-R. Liu, Room-temperature cured hydrophobic epoxy/graphene composites as corrosion inhibitor for cold-rolled steel, Carbon, 2014, 66: 144-153.
- [9] M.L. Zheludkevich, J. Tedim, M.G.S. Ferreira, "Smart" coatings for active corrosion protection based on multifunctional micro and nanocontainers, Electrochimica Acta, 2012, 82: 314-323.
- [10] K.S. Novoselov, V.I. Fal, L. Colombo, P.R. Gellert, M.G. Schwab, K. Kim, A roadmap for graphene, Nature 2012, 490: 192–200.
- [11] Singh BP, Jena BK, Bhattacharjee S, Besra L. Development of oxidation and corrosion resistance hydrophobic graphene oxide-polymer composite coating on copper. Surf Coat Technol 2013. 232:475–481.
- [12] Yu, Z., et al., Preparation of graphene oxide modified by titanium dioxide to enhance the anti-corrosion performance of epoxy coatings. Surface and Coatings Technology, 2015. 276: 471-478.
- [13] Yu, Z., et al., Fabrication of graphene oxide–alumina hybrids to reinforce the anti-corrosion performance of composite epoxy coatings. Applied Surface Science, 2015. 351: 986-996.
- [14] L. Fedrizzi, W. Furbeth, F. Montemor, Self-healing properties of new surface treatments, European Federation of Corrosion Publications, Number 2011, 58.
- [15] Murphy, E.B. and F. Wudl, The world of smart healable materials. Progress in Polymer Science, 2010. 35(1-2): 223-251.
- [16] Snihirova, D., et al., Hydroxyapatite Microparticles as Feedback-Active Reservoirs of Corrosion Inhibitors. ACS Applied Materials & Interfaces, 2010. 2(11): 3011-3022.
- [17] Buchheit, R.G., et al., Active corrosion protection and corrosion sensing in chromate-free organic coatings. Progress in Organic Coatings, 2003. 47(3–4): 174-182.
- [18] Zheludkevich, M.L., et al., Active protection coatings with layered double hydroxide nanocontainers of corrosion inhibitor. Corrosion Science, 2010. 52(2): 602-611.
- [19] Frederico Maia, Joao Tedim, Aleksey D. Lisenkov, Andrei N. Salak, Mikhail L. Zheludkevichnd M_ario G. S. Ferreira. Silica nanocontainers for active corrosion protection. Nanoscale, 2012, 4: 1287.
- [20] N. Pirhady Tavandashti, S. Sanjabi. Corrosion study of hybrid sol-gel coatings containing boehmite nanoparticles loaded with cerium nitrate corrosion inhibitor. Progress in Organic Coatings, 2010, 69:384-391.
- [21] He, Y., et al., Synthesis and properties of iron oxide coated carbon nanotubes hybrid materials and their use in epoxy coatings. Polymers for Advanced Technologies, 2015. 26(4): 414-421.
- [22] S.M. Megalai, P. Manjula, K.N. Manonmani, N. Kavitha, N. Baby, Metronidazole: A Corrosion Inhibitor for Mild Steel in Aqueous Environment, Portugaliae Electrochimica Acta, 2012, 30: 395-403.
- [23] O.R. Hummer W, Preparation of graphitic oxide J Am Chem Soc, 1958, 6: 1399.
- [24] C. Botas, P. Álvarez, P. Blanco, M. Granda, C. Blanco, R. Santamar á, L.J. Romasanta, R. Verdejo, M.A. López-Manchado, R. Menéndez, Graphene materials with different structures prepared from the same graphite by the

- Hummers and Brodie methods, Carbon, 2013, 65: 156-164.
- [25] J. Xu, C. Xiao, X. He, Controllable synthesis of a novel poly(vinyl alcohol)-based hydrogel containing lactate and PEG moieties, Polymer Engineering & Science, 2014, 54: 1366-1371.
- [26] T. Nakamura, X. Chu, T. Shimasaki, M. Shibata, Organogelation behavior and thermal properties of supramolecular polymer network composed of carboxy- and pyridyl-terminated 4-arm star-shaped epsilon-caprolactone oligomers, Journal of colloid and interface science, 2013, 404: 8-15.
- [27] H. Yi, C. Chen, F. Zhong, Z. Xu, Preparation of aluminum oxide-coated carbon nanotubes and the properties of composite epoxy coatings research, High Performance Polymers, 2013, 26: 255-264.
- [28] J. Vogelsang, W. Strunz, New interpretation of electrochemical data obtained from organic barrier coatings, Electrochimica Acta, 2001, 46: 3817-3826.
- [29] V.K. Singh, K. Pal, D.K. Pradhan, K. Pramanik, Castor oil and sorbitan monopalmitate based organogel as a probable matrix for controlled drug delivery, Journal of Applied Polymer Science, 2013, 130: 1503-1515.
- [30] J. Yuan, M.H. Liu, Chiral molecular assemblies from a novel achiral amphiphilic 2-(heptadecyl) naphtha 2,3 imidazole through interfacial coordination, Journal of the American Chemical Society, 2003, 125: 5051-5056.
- [31] Petersen, H.I., P. Rosenberg, and H.P. Nytoft, Oxygen groups in coals and alginite-rich kerogen revisited. International Journal of Coal Geology, 2008. 74(2): 93-113.
- [32] Deng, M., et al., Synthesis and Characterization of Biodegradable Poly(ester amide)s with Pendant Amine Functional Groups and In Vitro Cellular Response. Biomacromolecules, 2009. 10(11): 3037-3047.
- [33] Wang, N., et al., Adsorption of environmental pollutants using magnetic hybrid nanoparticles modified with β -cyclodextrin. Applied Surface Science, 2014. 305: 267-273.
- [34] J. Yuan, M.H. Liu, Chiral molecular assemblies from a novel achiral amphiphilic 2-(heptadecyl) naphtha 2,3 imidazole through interfacial coordination, Journal of the American Chemical Society, 2003, 125: 5051-5056.
- [35] Q. Shao, J. Tang, Y. Lin, J. Li, F. Qin, J. Yuan, L.-C. Qin, Carbon nanotube spaced graphene aerogels with enhanced capacitance in aqueous and ionic liquid electrolytes, Journal of Power Sources, 2015, 278: 751-759.
- [36] Chen, J., et al., An improved Hummers method for eco-friendly synthesis of graphene oxide. Carbon, 2013. 64: 225-229.
- [37] J. Chen, B. Yao, C. Li, G. Shi, An improved Hummers method for eco-friendly synthesis of graphene oxide, Carbon, 2013, 64: 225-229.
- [38] Gao, W., et al., New insights into the structure and reduction of graphite oxide. Nat Chem, 2009. 1(5): 403-8.
- [39] Park, K.-W. and J.H. Jung, Spectroscopic and electrochemical characteristics of a carboxylated graphene ZnO composites. Journal of Power Sources, 2012. 199: 379-385.
- [40] Sun, W., et al., Inhibiting the Corrosion-Promotion Activity of Graphene. Chemistry of Materials, 2015. 27(7): 2367-2373.
- [41] Sathiyanarayanan S, Azim SS, Venkatachari G. Corrosion protection coating containing polyaniline glass flake composite for steel. Electrochim Acta 2008, 53 (5):2087–2094.
- [42] Jadhav N, Vetter CA, Gelling VJ. The effect of polymer morphology on the performance of a corrosion inhibiting polypyrrole/aluminum flake composite pigment. Electrochim Acta 2013, 102: 28–43.
- [43] Nematollahi M, Heidarian M, Peikari M, Kassiriha SM, Arianpouya N, Esmaeilpour M. Comparison between the effect of nanoglass flake and montmorillonite organoclay on corrosion performance of epoxy coating. Corros Sci 2010; 52 (5):1809–1817.